GEOCHEMISTRY

Survival of presolar *p*-nuclide carriers in the nebula revealed by stepwise leaching of Allende refractory inclusions

Bruce L. A. Charlier[1]*†, François L. H. Tissot[2,3]†, Hauke Vollstaedt[4], Nicolas Dauphas[5], Colin J. N. Wilson[1], Ren T. Marquez[2]

The ^{87}Rb-^{87}Sr radiochronometer provides key insights into the timing of volatile element depletion in planetary bodies, yet the unknown nucleosynthetic origin of Sr anomalies in Ca-Al–rich inclusions (CAIs, the oldest dated solar system solids) challenges the reliability of resulting chronological interpretations. To identify the nature of these Sr anomalies, we performed step-leaching experiments on nine unmelted CAIs from Allende. In six CAIs, the chemically resistant residues (0.06 to 9.7% total CAI Sr) show extreme positive μ^{84}Sr (up to +80,655) and ^{87}Sr variations that cannot be explained by decay of ^{87}Rb. The extreme ^{84}Sr but more subdued ^{87}Sr anomalies are best explained by the presence of a presolar carrier enriched in the *p*-nuclide ^{84}Sr. We argue that this unidentified carrier controls the isotopic anomalies in bulk CAIs and outer solar system materials, which reinstates the chronological significance of differences in initial ^{87}Sr/^{86}Sr between CAIs and volatile-depleted inner solar system materials.

INTRODUCTION

Of the refractory elements enriched in calcium-aluminum–rich inclusions [CAIs; the oldest dated solids in the solar system: ~4.567 billion years (Ga)] (*1*, *2*), strontium (Sr) holds a central place because its isotopic composition is controlled by three fundamentally different processes: (i) mixing of presolar carriers with distinct isotopic composition, (ii) radiogenic ingrowth of ^{87}Sr from the decay of ^{87}Rb, and (iii) mass-dependent isotope fractionation and/or resetting via physico-chemical processes. Hence, Sr can provide constraints on the origins of CAIs [e.g., (*3*, *4*)], the genetic relationship between solar system materials [e.g., (*4*–*10*)], the chronology of volatile element depletion in planetary bodies (*11*–*13*), and nebular, accretion, and alteration processes that shaped the solar system (*3*, *4*, *14*–*16*). Because Rb is rather volatile while Sr is more refractory, the ^{87}Rb-^{87}Sr isotopic system is, in principle, one of the most powerful tools available to date the timing of volatile element depletion. In practice, however, many uncertainties remain due to the presence of nucleosynthetic anomalies in CAIs, meteorites and planetary materials, and the extent to which ^{87}Sr/^{86}Sr variations stem from ^{87}Rb decay or incomplete homogenization of nucleosynthetic anomalies.

The existence of Sr nucleosynthetic anomalies in CAIs and their host meteorites, relative to Earth, is well documented (*4*–*7*, *9*, *10*, *13*, *17*, *18*). These positive anomalies are on the order of a few tens to hundreds of parts per million and usually expressed in the μ^{84}Sr notation: the deviation in parts per million from the measured NBS-987 value after internal normalization to a constant ^{86}Sr/^{88}Sr = 0.1194. Despite the apparent ^{84}Sr excesses seen in internally normalized data, it remains unclear whether the anomalies observed in bulk CAIs result

from variations in the *p*-nuclide ^{84}Sr or reflect (through internal normalization) an *r*-process anomaly in ^{88}Sr [e.g., (*7*, *19*)]. Either interpretation is possible and is an enduring challenge in Sr isotopic studies of early solar system materials.

This uncertainty surrounding the nature of the ^{84}Sr anomalies has implications beyond unraveling the presolar heritage of the solar system. In particular, it affects dating of volatile element depletion in the early solar system. Because Rb is more volatile than Sr (50% condensation temperatures under solar nebula conditions of 800 and 1464 K, respectively) (*20*), one can constrain the timing of the evaporation/condensation event(s) that lead to the depletions in moderately volatile elements observed in planetary bodies (*5*, *11*–*13*, *21*), which depends on the assumptions (i) that the initial ^{87}Sr/^{86}Sr ratio of solar system materials is known and homogeneous and (ii) that ^{87}Sr/^{86}Sr variations are entirely due to ^{87}Rb decay. These assumptions may not be warranted if isotopic anomalies of presolar origin are present in the nascent solar system and incompletely homogenized. Indeed, to correct for instrumental mass-dependent fractionation during analysis, calculations of ^{87}Sr/^{86}Sr use an internal normalization scheme by setting the ^{86}Sr/^{88}Sr ratio to a fixed value. If the nucleosynthetic anomalies in CAIs and bulk solar system materials reside in the *p*-nuclide ^{84}Sr [as proposed in (*4*, *6*, *7*, *22*, *23*)], then the normalization is warranted and so are the chronological interpretations based on variable initial ^{87}Sr/^{86}Sr ratios. If, however, the anomalies lie on ^{86}Sr (*s*-deficit) or ^{88}Sr (*r*-excess), the normalization will shift the initial ^{87}Sr/^{86}Sr ratio (*5*), and variations in initial ^{87}Sr/^{86}Sr would instead reflect the compounded effect of radiogenic ingrowth and nebular isotopic heterogeneity (*9*, *13*, *17*).

These outstanding questions can be answered, provided that one finds materials that (i) formed early in the history of the solar system and (ii) were minimally affected by radiogenic ingrowth of ^{87}Sr. As the oldest materials formed in the solar system, CAIs are the prime target for such investigations. Yet, finding CAIs with pristine, low Rb/Sr ratios is nontrivial because Rb (and to a lesser extent Sr) are fluid-mobile, and the Rb-Sr systematics in CAIs can be significantly disturbed during aqueous alteration [e.g., (*4*, *17*, *24*)]. Here, in an effort to isolate phases with low Rb/Sr ratios and constrain the nature of the carrier of ^{84}Sr anomalies, we subjected to a step-leaching

[1]School of Geography, Environment and Earth Sciences, Victoria University of Wellington, Wellington 6140, New Zealand. [2]The Isotoparium, Division of Geological and Planetary Sciences, California Institute of Technology, Pasadena, CA 91125, USA. [3]Department of the Earth, Atmospheric and Planetary Sciences, Massachusetts Institute of Technology, Cambridge, MA 02139, USA. [4]Thermo Fisher Scientific, Hanna-Kunath-Str. 11, 28199 Bremen, Germany. [5]Origins Laboratory, Department of the Geophysical Sciences and Enrico Fermi Institute, The University of Chicago, 5734 South Ellis Avenue, Chicago, IL 60637, USA.
*Corresponding author. Email: bruce.charlier@vuw.ac.nz
†These authors contributed equally to this work.

dissolution protocol a suite of nine fine-grained CAIs (fg-CAIs) from Allende (see Table 1 for listing and figs. S1 to S9 for imagery). The fg-CAIs were chosen for their relatively primitive characteristics. In general, they display condensate-like petrographic features (*25*), have never been melted, and their chemical compositions match those predicted by equilibrium thermodynamic calculation for partial condensation from a gas of solar composition gas [e.g., (*26–29*)]. Our samples (figs. S1 to S9) share these features, and, in particular, their Rare Earth Elements (REE) patterns are classic type II volatility-controlled patterns (fig. S10 and table S1). Because in situ methods would provide insufficient precision, the isolation of pristine domains (i.e., with low primary Rb/Sr ratios) was performed chemically via step leaching.

The Sr isotopic compositions of an unleached powder aliquot (i.e., bulk analysis) and each leached fraction were measured by thermal ionization mass spectrometry (TIMS) using internally normalized and double-spike methodologies. After visual inspection of slabs of the Allende CV chondrite, CAIs with fine-grained morphologies were extracted using clean steel dental tools (see Materials and Methods below). Given the limited mass of the samples (13 to 158 mg), and to ensure sufficient precision even on the smallest sample fractions (<10% of total Sr in the CAI), 10^{13}-ohm feedback resistors (*30*) were used as these permitted high-precision Sr measurements on load sizes as low as 150 pg. Each leachate fraction was split into three aliquots to quantify (i) nucleosynthetic anomalies through internal normalization on an unspiked sample aliquot, (ii) stable ^{86}Sr and ^{88}Sr relationships using double-spike methodologies, and (iii) ^{87}Rb abundances by high-sensitivity inductively coupled plasma mass spectrometry (ICP-MS) measurements to assess the contribution of ^{87}Rb-decay on $^{87}Sr/^{86}Sr$ variations and estimate initial $^{87}Sr/^{86}Sr$ values using Rb-Sr isochrons. At each stage of the step-leaching process, the leached residues were weighed to estimate (i) the amounts of components dissolved and (ii) their chemical and Sr isotopic composition.

RESULTS
Step-leaching methodology and Sr release patterns
Each CAI sample was subjected to a five-step leaching protocol (see Materials and Methods) of increasingly aggressive acid type and molarity, and temperature. The leaching experiments and separation of the aliquots for internally normalized measurements were performed before any Sr double-spike materials were used in the laboratory (see the Supplementary Materials for details). Of the nine CAIs analyzed (Table 1), only one (*Logan*) had no material remaining after the fourth leaching step. In all cases, the first three leach steps contained >80% of the total Sr budget, and the amount of Sr released in each step typically decreased by two to three orders of magnitude across the total experiment (Fig. 1 and Supplementary Materials). To test the efficiency of the step-leaching protocol and accuracy of the gravimetric accounting for Rb and Sr yields, a separate fraction of powder from each CAI was dissolved in bulk, using a Parr bomb to ensure total dissolution, and analyzed similarly to the leach aliquots. Excellent agreement was observed between the Sr isotopic characteristics (Fig. 2) for the bulk samples versus the gravimetrically summed leach fractions.

Standard data
Two instruments were used in this work: the 10^{11}-ohm equipped Triton TIMS at Victoria University of Wellington (VUW), which was used for large Sr loads (100 to 1000 ng), and the 10^{13}-ohm equipped Triton XT at the Thermo Fisher factory in Bremen, which was used for Sr loads below 100 ng. Data accuracy was thoroughly evaluated on both instruments (see Materials and Methods). External reproducibility for internally normalized data on the VUW Triton was (2 SD, $n = 9$; 900 ng Sr loads): $^{84}Sr/^{86}Sr = 0.0564888 \pm 12$ [22 parts per million (ppm)] and $^{87}Sr/^{86}Sr = 0.7102604 \pm 42$ (5.9 ppm). External reproducibility on the Bremen instrument was evaluated for Sr loads of 1 ng, 500 pg, and 50 pg (fig. S11). The average ($n = 10$) $^{84}Sr/^{86}Sr$ ratio and 2 SD values were found to be, respectively, 0.0564997 ± 171 (302 ppm), 0.0564977 ± 180 (326 ppm), and 0.0564966 ± 1280 (2265 ppm). The average $^{87}Sr/^{86}Sr$ and 2 SD values were, respectively, 0.710260 ± 45 (64 ppm), 0.710248 ± 43 (60 ppm), and 0.710234 ± 150 (211 ppm) (table S2).

Similar tests performed on double-spike measurements [used to constrain mass fractionation effects, using methods from (*8*)] yielded external reproducibilities (2 SD) on the VUW instrument (900-ng loads, $n = 8$) of ±0.038 per mil (‰) and ± 0.030‰ for $\delta^{84}Sr/^{86}Sr$ and $\delta^{88}Sr/^{86}Sr$, respectively. Using the same double-spike methodologies for 1-ng loads on the Bremen instrument yielded external reproducibilities of ±0.29 and ±0.19‰ for $\delta^{84}Sr/^{86}Sr$ and $\delta^{88}Sr/^{86}Sr$, respectively ($n = 10$).

Strontium isotopic release patterns
Nucleosynthetic anomalies
The internally normalized $^{84}Sr/^{86}Sr$ data in each leach step (expressed as $\mu^{84}Sr$; see the "Notations" section in Materials and Methods) are shown in Fig. 1. Within each CAI, wide variations are observed. In all cases, $\mu^{84}Sr$ values are positive, and the first three leaching steps (80 to 99% total Sr) have elevated $\mu^{84}Sr$ values that are within the range of published values observed in bulk single CAIs (Fig. 2). In contrast, the final leach (L4) and residue digest (L5) show $\mu^{84}Sr$ anomalies reaching per mil to percent levels, and the fractions most depleted in Sr also display the largest anomalies (Fig. 1). The largest anomaly was found in *Hank*, where the final digest (L5) revealed an extreme $\mu^{84}Sr$ value of 80,655 ± 1807.
Rb/Sr systematics and initial $^{87}Sr/^{86}Sr$ ratios
The values for both $^{87}Rb/^{86}Sr$ and measured $^{87}Sr/^{86}Sr$ (Fig. 3) cover extreme ranges (e.g., $^{87}Sr/^{86}Sr$ measured for *Logan* in L1 of 0.936) and show three important features. (i) The $^{87}Rb/^{86}Sr$ relationships remain consistent across the first four leach steps, with ages and

Table 1. Sample names and masses of CAI samples.

Name	Catalog number	Sample mass for leaching experiments (mg)	Sample mass for bulk measurements (mg)
Charles	4290-FG-1	104.46	6.1278
Erik	4299-FG-1	53.63	4.0692
Hank	4317-FG-1	15.44	1.4106
Jean	4321-FG-1	20.33	3.1293
Logan	4321-FG-2	12.83	2.9271
Ororo	4322-FG-1	157.85	7.9512
Peter	5047-C2/D2-FG-1	25.52	2.5550
Raven	5058-FG-1	47.17	7.0199
Scott	5064-FG-2	54.88	7.5929

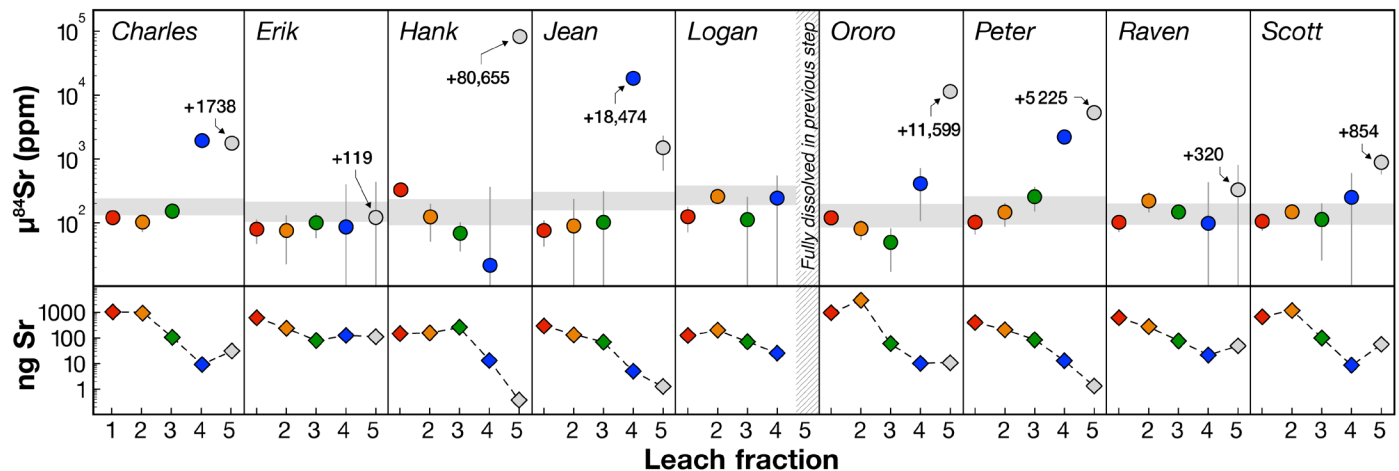**Fig. 1. μ^{84}Sr values and associated Sr yields from step leaching.** Top: Internally normalized μ^{84}Sr for each leach fraction (table S4). The gray shaded bar represents the measured isotopic composition of the bulk CAI ($\pm$2 SD). Bottom panels show the amount of Sr (ng) released in each leaching step. Note the use of log-scales throughout. See Table 1 for the CAI catalog numbers.

initial ^{87}Sr/^{86}Sr values overlapping within uncertainty (Fig. 3), despite the Rb abundances and Rb/Sr ratios in the first three leach fractions diminishing between each step. The mean square of weighted deviates (MSWD; equivalent to the reduced χ^2) values for the best-fit lines for steps L1 to L4 are such, however, that some scatter beyond analytical error is present. (ii) Minor amounts of Rb persist into leaching step L4, with a similarly consistent pattern of correlation with ^{87}Sr/^{86}Sr measured ratios, and yield a precise initial ratio for L4 of 0.698784 $\pm$ 76 (2 SD). (iii) In marked contrast to the earlier leach steps, the ^{87}Rb/^{86}Sr versus ^{87}Sr/^{86}Sr relationships of the L5 residual refractory phases are incoherent. In all but one case (L5_Raven), the data scatter to more radiogenic ^{87}Sr/^{86}Sr values than the L4 isochron and show no meaningful age relationships.

A complementary view of the data can be obtained by plotting individual isochrons across all leach steps for each CAI separately (fig. S12). Plotted in this fashion, the leach steps define best-fit lines that are heavily leveraged by L1, but most yield ages within error of the solar system age. The scatter in the model ages and high MSWD values in Fig. 3 and fig. S12 imply that other effects are present. There may be a second-order influence from minor incongruent mineral dissolution induced by the step leaching process. Later-stage asteroidal alteration also cannot be ruled out with the available data. Other components within the same fragment of Allende would need to be analyzed in the same fashion to search for consistency that would indicate alteration in the meteorite parent body. Initial ^{87}Sr/^{86}Sr ratios range between 0.6967 $\pm$ 73 and 0.6994 $\pm$ 12 (fig. S12). These initial ^{87}Sr/^{86}Sr ratios are consistent within error and define a weighted mean of 0.69874 $\pm$ 11 (MSWD = 0.23), which agrees within error with the value obtained above by grouping the L4 data points across all nine CAIs.

Stable isotope fractionation patterns

The stable Sr isotopic compositions derived from the double-spike methodologies are plotted on $\delta^{88/86}$Sr versus $\delta^{84/86}$Sr three isotope plots in Fig. 4. For all but one sample (Hank), the leach fractions L1 to L3 define tight clusters in the three-isotope plots (Fig. 4B), with leach fractions L4 and L5 showing distinct compositions. The location of the clusters defined by the L1 to L3 fractions scatter between a CAI mass-dependent fractionation line (MDFL) defined from bulk

CAI data (4), which is offset by 0.144‰ in the $\delta^{84/86}$Sr coordinate, and the equilibrium MDFL (Fig. 4A). The CAI MDFL is also identical, within error, to that previously defined by primitive meteorites (8). The CAI data presented here cover a total range of $\delta^{88/86}$Sr values from −1.94 to +1.14‰ and lie within the range of the values previously obtained for bulk CAIs (~5.3‰ in $\delta^{88/86}$Sr, from −3.67 to +1.67‰) (4). In stark contrast, the range of $\delta^{84/86}$Sr values from steps L4 and L5 shows clear positive departure from both the terrestrial and bulk CAI MDFLs, in some cases, to extreme values never before observed (up to $\delta^{84/86}$Sr = 81.41 $\pm$ 2.49‰).

DISCUSSION

Bulk CAI versus individual leachates Sr data

The nucleosynthetic, radiogenic, and stable "bulk" CAI data obtained in this work (reconstructed from the individual masses and isotopic characteristics of materials at each leach step) are all in good agreement with literature data obtained on dissolutions of bulk CAI samples (4, 6, 9, 10, 13, 17, 18), indicating that the samples investigated here are representative of the type of CAIs previously studied at the bulk level (fine-grained group II). The step leaching protocol used here, however, provides insights into the history and isotopic heritage of CAIs that shed new light on bulk isotopic data.

There is a general consistency of Sr isotopic signatures (μ^{84}Sr, $\delta^{84/86}$Sr, $\delta^{88/86}$Sr, and initial ^{87}Sr/^{86}Sr ratios) across the first three leaching steps (L1 to L3; e.g., Figs. 2 and 4), which together account for most of the Sr inventory of the bulk samples (80 to 99%). In three-isotope plots, the double-spike data ($\delta^{84/86}$Sr and $\delta^{88/86}$Sr) for fractions L1 to L3 cluster tightly (Fig. 4B), suggesting that either (i) a single phase is being digested in all three steps, or (ii) the different phases digested in these steps experienced the same extent of Sr mass-dependent fractionation. Major and trace element concentrations obtained on each leachate show that multiple phases are being digested in each step (fig. S13), starting with secondary phases like sodalite and nepheline in L1 and L2, followed by the digestion of hedenbergite, grossular, and some primary phases like melilite and diopside in L3, L4, and lastly the most refractory phases like spinel in L4 and L5, and other trace phases in L5. Yet, because fg-CAIs
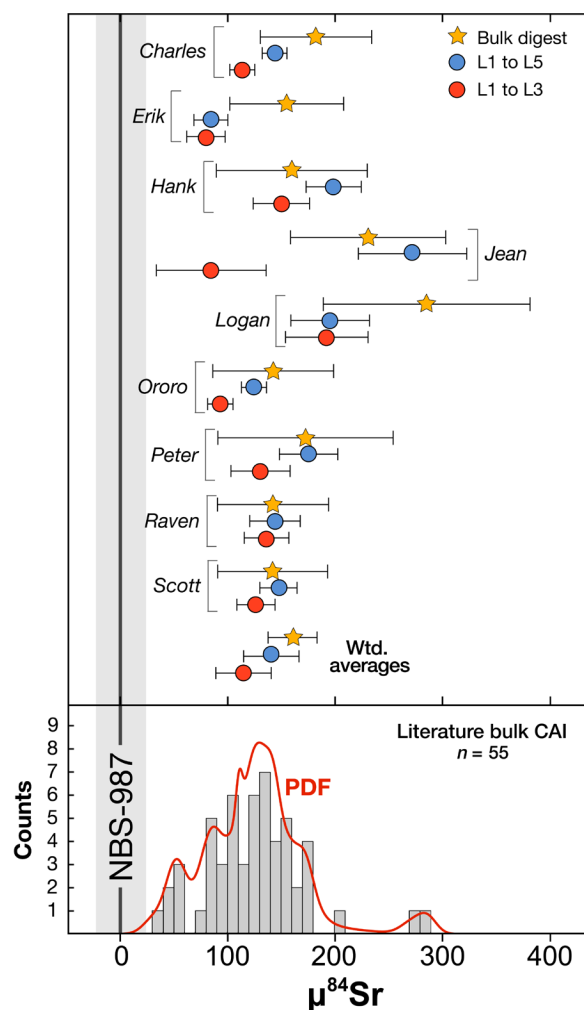
Fig. 2. Summary of $\mu^{84}Sr$ data presented in this paper. Top: Recombined estimates for $\mu^{84}Sr$ for steps L1 to L3 (red circles) and L1 to L5 (blue circles) are compared to the bulk data for each CAI. The gray-shaded bar represents the external reproducibility of 22 ppm (2 SD) obtained in this study for the internally normalized $\mu^{84}Sr$ for 1000-ng loads of the NBS-987 standard (table S1). Weighted averages were calculated using Isoplot (61). Bottom: Relative probability distribution function (PDF) (using Isoplot) (61) and histogram for all published Allende bulk CAI $\mu^{84}Sr$ data for comparison [incorporating data from (4, 6, 9, 10, 13, 17, 18)].

have condensate textures, one would not necessarily expect the different phases digested in steps L1 to L3 to be characterized by a similar extent of mass fractionation, at least as a primary feature. Because Allende is known to have been subjected to intense aqueous alteration, which is the most likely source of the high Rb content seen in L1 and L2, the similar $\delta^{84/86}Sr$ and $\delta^{88/86}Sr$ values in L1 to L3 could be the result of closed-system Sr redistribution and homogenization during aqueous alteration. This is consistent with the predominantly secondary nature of the phases digested in leachates L1 to L3 and the generally homogeneous $\mu^{84}Sr$ values in these leachates, which are similar to the values in both fg- and coarse-grained bulk CAIs ($\mu^{84}Sr = $ ~+125) (4). Furthermore, Allende as a whole has a $\mu^{84}Sr$ value of +58 ± 17 (7), and the matrix alone should have an even lower $\mu^{84}Sr$ value (to satisfy mass balance requirements). If

extraneous Sr from the meteorite matrix had been introduced in the CAIs during parent body alteration, this would have lowered the $\mu^{84}Sr$ value of the most fluid mobile component of the CAIs relative to the refractory components that are not sampled by leachates L1 to L3. We therefore conclude that, although aqueous alteration partially homogenized the Sr isotopic composition of the CAIs, it did not mobilize Sr beyond the boundaries of the CAIs and thus each CAI can be treated as an individual closed system object.

The final leachate (L4; 0.25 to 10.6% of total Sr) and residue digest (L5; 0.06 to 9.7% of total Sr), which together concentrate the chemically resistant phases, show Sr isotope systematics in stark contrast of those observed in the initial leachates. In particular, these leachates display positive $\mu^{84}Sr$ anomalies of unprecedented magnitude, up to +80,655 ± 1807 in the *Hank* CAI (Fig. 1). In Fig. 2, we compare the bulk CAI $\mu^{84}Sr$ values with those reconstructed by mass balance by taking into consideration the $\mu^{84}Sr$ values and Sr amounts in each leachate fraction. We find agreement between the bulk value and the reconstituted value from L1 to L5. While the Sr amounts in L4 and L5 are small, they contribute significantly to bulk $\mu^{84}Sr$ anomalies, and not considering them would lead to a discrepancy between measured and reconstructed bulk $\mu^{84}Sr$ anomalies. This comparison between measured and reconstructed bulk $\mu^{84}Sr$ values shows that the anomalies measured in L4 and L5 are real and not analytical artifacts due to the low amounts of Sr available for isotopic analysis in those leachates. These data demonstrate the existence and survival in CAIs of isotopically exotic materials, which have here been concentrated through our chemical step-leaching protocol.

A *p*-process origin for ^{84}Sr excesses in CAIs

Whether the nucleosynthetic anomalies seen in CAIs and planetary bodies are due to variations in the *p*-nuclide (^{84}Sr) or *r*-nuclide (^{88}Sr) is a matter of contention [e.g., (4–10, 13, 17)]. If the positive $\mu^{84}Sr$ values measured here were the result of *r*-process excesses in ^{88}Sr propagating to ^{84}Sr as an internal normalization (to $^{86}Sr/^{88}Sr = 0.1194$) artifact, this would also result in apparent negative ^{87}Sr shifts of a magnitude half those of ^{84}Sr (i.e., the samples should appear less radiogenic) (5). Despite the large $\mu^{84}Sr$ values in fractions L4 and L5, no negative ^{87}Sr anomalies are seen in those fractions. The data from leach step L4 show coherent behavior (Fig. 3D), yielding an initial $^{87}Sr/^{86}Sr$ value of 0.698784 ± 0.000076 (2 SD, MSWD = 9.2) that lies within the error of the original ALL value of 0.69877 ± 0.00004 reported by Gray *et al.* (24) for Allende CAI USNM 3898 [see also (31)]. Similarly, a range of low apparent $^{87}Sr/^{86}Sr$ initial ratios can be calculated for the individual age-corrected analyses in L4 ($^{87}Sr/^{86}Sr = $ 0.698587, L4_*Ororo* to 0.698883, L4_*Jean*), which, in turn, agree with those presented by Amelin *et al.* (32) for the leachates of the FUN (fractionation and unknown nuclear effects) CAI, CMS-1 ($^{87}Sr/^{86}Sr = $ 0.69839 to 0.69900). Furthermore, despite the large $\mu^{84}Sr$ values in leach step L5, no accompanying negative ^{87}Sr anomalies are seen in those fractions, as all but one sample (*Raven*) plot significantly above the best-fit reference line for step L4 $^{87}Sr/^{86}Sr$ values (Fig. 3). These results are inconsistent with the anomalies stemming from any substantive *r*-/*s*-process ^{88}Sr variability and instead imply that the anomalies lie primarily in the *p*-nuclide ^{84}Sr.

The double-spike data further support this conclusion. In the three-isotope plots (Fig. 4), the data for fractions L4 and L5 form a horizontal envelope (displacement toward higher $^{84}Sr/^{86}Sr$ ratios), which strongly argues against any notion that the $\mu^{84}Sr$ variations are an artifact of normalization to an inaccurate value for the $^{88}Sr/^{86}Sr$ ratio.
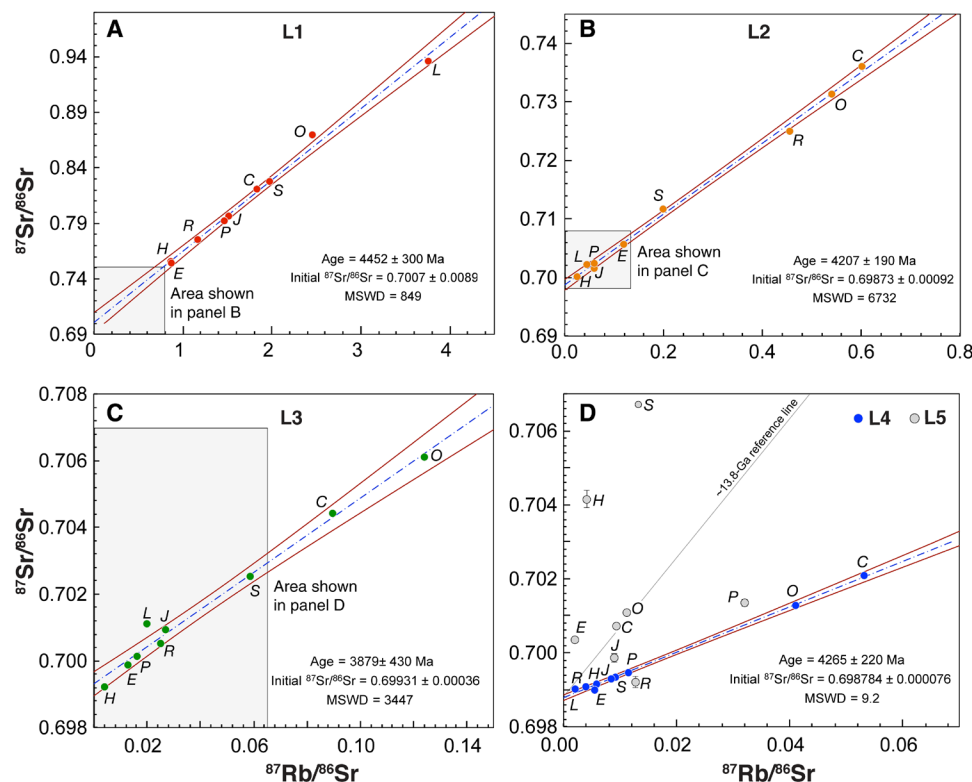
Fig. 3. (A-D) ^{87}Sr/^{86}Sr versus ^{87}Rb/^{86}Sr values for each leach fraction. Panels are scaled in each case to show a suitable range in values on the *x* and *y* axes. In (D), analyses from leach steps 4 and 5 are filled blue and gray symbols, respectively. Shaded box in each panel represents the area shown in each successive panel for comparison. Error bars are smaller than symbol size unless shown. Best-fit lines and 2 SD error envelopes are calculated using the model 3 fit of Isoplot (which assumes that the scatter is due to a combination of assigned errors plus a normally distributed variation in the *y* value) (*61*) and an ^{87}Rb decay constant of 1.3971 × 10^{-11} year^{-1} (*62*). A ~13.8-Ga reference line has been added to illustrate that several of the L5 aliquots have extreme and unsupported ^{87}Sr/^{86}Sr ratios, emphasizing their exotic nature with respect to solar system materials. For comparison, isochron diagrams constructed based on all the leachates from each of the individual CAIs are shown in fig. S11.

Any hypothetical variability in the ^{88}Sr/^{86}Sr ratio resulting from the proportions in *r*- versus *s*-process ^{88}Sr may be discerned in individual L4-L5 data pairs but is wholly subordinate to the $\delta^{84/86}$Sr variations. This is demonstrated in Fig. 4B by the nearly horizontal slopes of hypothetical tie lines for those pairs showing extreme $\delta^{84/86}$Sr values, and the fact that no L5 analyses fall outside the range of $\delta^{88/86}$Sr values for the dataset (L1 to L4 and, by definition, reconstituted bulk samples) as a whole. In addition, the vertical trajectory of the L4 and L5 data in a plot of μ^{84}Sr versus ^{87}Sr/^{86}Sr (Fig. 5) precludes the presence of any discernible ^{88}Sr excess, which would drive the data to less radiogenic values for ^{87}Sr/^{86}Sr.

The unsupported ^{87}Sr in the L5 fraction (i.e., ^{87}Sr excesses that cannot be accounted for by in situ decay of ^{87}Rb) further emphasizes the exotic nature of the carrier concentrated by the step leaching protocol. Although a broad correlation is observed between the μ^{84}Sr versus ^{87}Sr/^{86}Sr (corrected or uncorrected for radiogenic ingrowth based on the Rb/Sr of the sample fraction; Fig. 5), the origin of the ^{87}Sr excesses remains unclear. These could reflect (i) incongruent dissolution and fractionation of Rb/Sr, (ii) nucleosynthetic anomalies in ^{87}Sr, (iii) radiogenic decay of ^{87}Rb in the interstellar medium and incorporation into the presolar carriers, or (iv) contamination on the parent body with radiogenic Sr. None of these explanations can be ruled out at this point, because both the ages and initial ratios of these materials are unknown.

Nature, abundance, origin, and preservation of presolar carriers in CAIs

A long-held view is that presolar grains are only present in the fine-grained matrices of primitive meteorites that have experienced minimal high-temperature alteration or melting (*33, 34*), and CAIs, which formed at high temperature, should be thus devoid of presolar grains (*35*). In contrast with this general view, but in agreement with a recent stepwise pyrolysis study of noble gas isotopic signatures in fg-CAIs from Allende (*36*), our data provide evidence for the survival of distinct presolar carriers in CAIs. On the basis of the specific krypton, neon, and xenon *s*-process excesses observed, Pravdivtseva *et al.* (*36*) proposed that the carriers isolated in the 1200° to 1300°C pyrolysis step were presolar SiC (<0.2 μm in size), which were incorporated in fg-CAIs during their formation and survived any secondary processing. Although our data do not permit identification of the specific carrier(s) of the ^{84}Sr anomalies, SiC grains are extremely unlikely candidates. ^{84}Sr excesses represent *p*-nuclide anomalies and the few SiC grains that have been measured for Sr isotopes (*n* = 39, including both grains from Asymptotic Giant Branch (AGB) stars and supernovae) display either solar composition or negative anomalies (down to −90.6 ± 2.0%) (*37–39*). No presolar grains, to date, have been found with excess ^{84}Sr signatures.

The *p*-nuclides are thought to be formed primarily by photodisintegration of progenitor isotopes when the temperature in stars
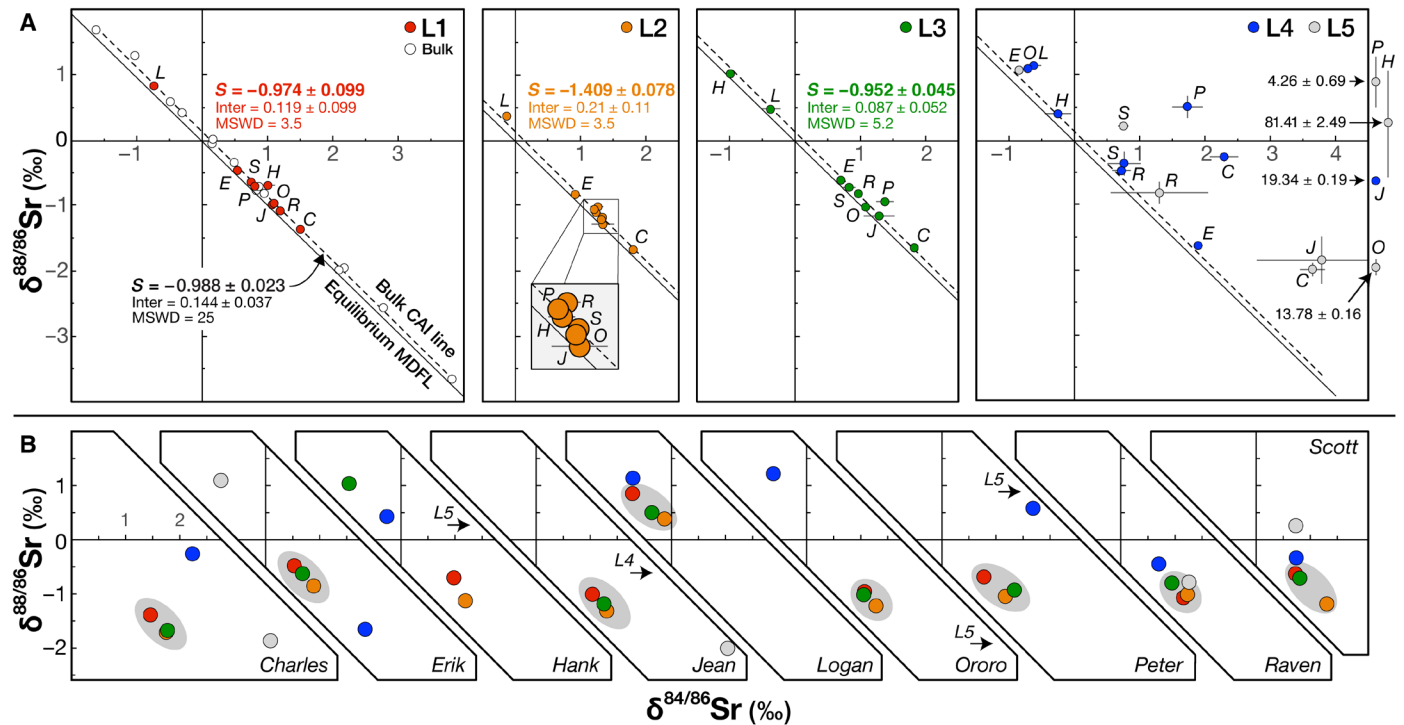
Fig. 4. $\delta^{88/86}$Sr versus $\delta^{84/86}$Sr (obtained using the double-spike technique). (**A**): Data for all CAIs organized by leach fraction. "Equilibrium MDFL" denotes the equilibrium mass-dependent fractionation line (solid line) that passes through the origin (the measured composition of NBS-987) with a slope of −0.978 (*14*). A best-fit line (dashed line) to the bulk CAI data from Charlier *et al.* (*4*) is plotted for comparison with the step leach data. The bulk CAI best-fit line is offset from the equilibrium MDFL by +0.144‰ in $\delta^{84/86}$Sr. 2 SD uncertainties are smaller than the symbol size unless shown. (**B**): Data for all leach fractions organized by CAI. For all CAIs except one (*Hank*), the data from leaching steps 1 to 3 are tightly clustered (shaded area), consistent with partial homogenization of the Sr isotopic composition of the CAIs during closed-system aqueous alteration (see the main text).
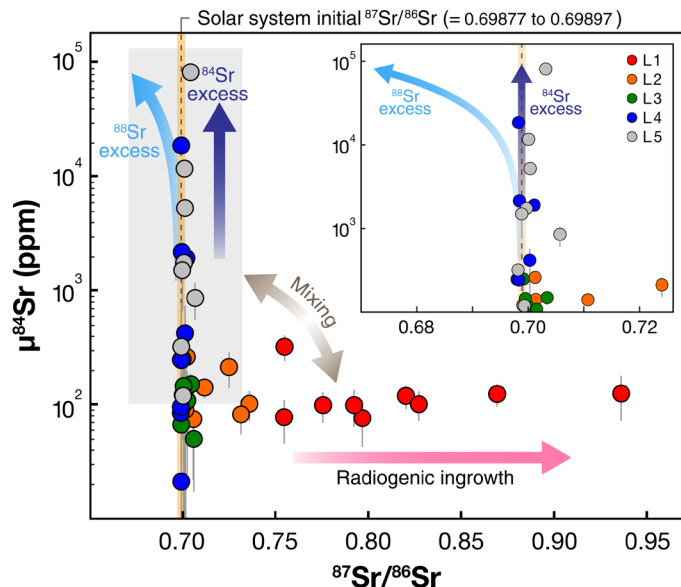

Fig. 5. Nucleosynthetic anomalies (μ^{84}Sr) versus ^{87}Sr/^{86}Sr, both from internally normalized data. Expected relationships for pure radiogenic ingrowth, ^{84}Sr excess and correlation arising from internal normalization to ^{88}Sr/^{86}Sr in the presence of *r*-process anomalies (arrows) are shown. Component mixing follows curved trajectories in such a frame of reference (they would follow straight lines if the *y* axis were on a linear scale). Shaded area denotes the region plotted on the inset figure.

reaches ~3×10⁹ K (*40*). Core collapse supernovae (*41*) and type Ia supernovae [e.g., (*42*)] are two likely sites of such process, yet in both cases, it is unclear whether grains would condense from those materials and, at least for type Ia supernovae, no grain condensation has been observed from spectroscopic observations. The only documented *p*-nuclide anomalies from presolar grains are in nanodiamonds, which upon heating release Xe with a Xe-HL (H and L stand for high and low mass isotopes, respectively) signature characterized by enrichment in both *p*- and *r*-process nuclides (*43*). The excesses in Sr *p*-nuclide without corresponding Sr *r*-process enrichments observed in our leach fractions L4 and L5 therefore point to the existence of presolar phases with only *p*-nuclide anomalies. These data, taken at face value, would indicate that at least two types of presolar grains (the *p*-nuclide–rich carrier and the SiC inferred from noble gas analyses) were incorporated and preserved in fg-CAIs.

The presence of presolar grains in CAIs, as evidenced by our Sr data and the noble gas data of Pravdivtseva *et al.* (*36*) is unexpected. Presolar grains would not be expected to survive either the high temperatures of the CAI forming region or the aqueous alteration and mild heating of the Allende parent body that destroyed some presolar grains (SiC) but not all (nanodiamonds) (*33*, *34*). How and when presolar grains were incorporated into Allende fg-CAIs, and how they survived, is therefore an important question. One possibility is that these presolar grains are not a primary feature of the CAIs but were introduced in these inclusions during aqueous alteration on the parent body. The large positive ^{84}Sr anomalies (maximum

$\mu^{84}Sr = +80655 \pm 1807$) observed in leach fractions L4 and L5 in our fg-CAIs argues, however, against such a scenario. These ^{84}Sr enrichments are unique to fg-CAIs and in stark contrast with the large negative anomalies (down to $\mu^{84}Sr = -4741 \pm 70$ in Murchison) in refractory residues of leaching experiments of most bulk carbonaceous chondrites (Ivuna, Murchison, and Tagish Lake) (6, 7, 10). These negative values are consistent with the high abundance of SiC grains in these meteorites (44), and their refractory nature would lead to concentration in the final steps of the leaching protocol. Furthermore, step-leaching of bulk Allende samples yielded essentially homogeneous, positive ^{84}Sr signatures in all leaching steps, identical to the bulk Allende value ($\mu^{84}Sr = \sim +58$) (7), consistent with the destruction of presolar grains during aqueous alteration, the homogenization of the Sr anomalies at the bulk Allende scale, and the low residual abundances of presolar grains in Allende (0.0062 ppm of SiC) compared to less altered carbonaceous chondrites (e.g., 13.5 ppm of SiC in Murchison) (44). The ^{84}Sr-rich nature of the presolar carrier in fg-CAIs is thus inconsistent with introduction of these grains during fluid alteration on the Allende parent body.

The presolar component(s) in fg-CAIs, represented by the residues in leach steps L4 and L5, therefore appear to be distinct and primary phases, having been incorporated in fg-CAIs during their genesis rather than introduced by secondary processes on the Allende parent body. In theory, the geochemical signatures of the successive leachates could shed light on the nature of these carrier phases. Cross-plots of major and trace element atomic ratios in the leachates do not, however, allow us to pin down the nature of the carriers. The contribution of the carriers to the chemical composition of the leachate is overwhelmed by those of the major phases (fig. S13), and the L5 leachates define mixing arrays between a spinel pole and an Al-rich diopside pole. Without further knowledge of the nature of these carriers, their survival through the alteration events experienced by the Allende CAIs could be explained if they occurred as inclusions within refractory minerals (i.e., for which they could have acted as nucleation seeds), were isolated from the fluid flow path by aggregates of the refractory minerals in fg-CAIs, or were in themselves resistant to alteration by the metasomatic fluids. The first scenario would imply survival of the presolar carrier in high-T environments where the CAI minerals condensed. The second requires condensation of the minerals forming fg-CAIs in high-T regions, then transport to cooler regions where the presolar carriers would be present (or cooling of the CAI forming region and introduction of the presolar carriers) before, lastly, accretion of the CAIs from condensed grains. The third scenario would rule out presolar carriers that are prone to destruction by parent body metamorphism (e.g., silicate grains) as the carrier phase of the ^{84}Sr excesses observed here.

Implications of *p*-process Sr anomalies in CAIs for the isotopic heritage of the solar system

The significant ^{84}Sr excesses from fractions L4 and L5 suggest that most of the apparent ^{84}Sr excesses in the bulk CAIs are due to one or more of the various *p*-processes (40). L4 and L5, which only contain 0.5% (*Ororo*) to 20.3% (*Erik*) of the total Sr inventory of the CAIs, contribute between 1.6% (*Logan*) and up to 69.7% (*Jean*) of the ^{84}Sr excesses of the bulk CAIs (Fig. 2). In particular, in the *Jean* CAI, which displays one of the larger reported anomalies in CAIs ($\mu^{84}Sr = +230$), L4 and L5 only account for 1.3% of the Sr inventory, but their influence on the bulk $\mu^{84}Sr$ value is dominant ($\mu^{84}Sr = +191$, 69.7% of the bulk anomaly).

Because the composition of many refractory elements in CAIs appears to be mainly controlled by variations in the relative contribution of the *r*- and *s*-process (Zr, Mo, Hf, W, and Nd), the same interpretation has often been assigned to Sr, Ba, and Sm anomalies [e.g., (18)]. However, the *p*-nuclides could represent up to 70 and 75% of the nucleosynthetic heritage of, respectively, Ba and Sm in bulk CAIs and all of the anomalies in Sr (45). A main control of *p*-processes on bulk CAI Sr anomalies, as shown by our data, means that the contribution of *p*-processes in setting the bulk CAI composition of Sm and Ba is possible and demands further investigation.

A *p*-process origin of Sr anomalies in CAIs also has ramifications for our understanding of the origin of the ^{84}Sr anomalies in bulk meteorites. Initially identified based on clustering of planetary materials in $\varepsilon^{50}Ti$, $\varepsilon^{54}Cr$, and $\Delta^{17}O$ isotope spaces (46), a clear isotopic dichotomy also exists in Sr isotopic characteristics between carbonaceous (CC) and non-carbonaceous (NC) objects (8). This dichotomy has also been documented in numerous other isotope systems and, in combination with elemental abundance data for both refractory and nonrefractory elements (Ti, Sr, Ca, Cr, Ni, Zr, Mo, Ru, Ba, Nd, Sm, Hf, W, and Os), reveals a general pattern whereby the CC reservoir is offset from the NC reservoir toward the composition of CAIs (10). This observation holds even for CC bodies where visible CAIs are extremely rare or absent (e.g., CI chondrites), implying the existence in CC materials of an as-yet unidentified (cryptic) refractory component, isotopically similar to CAIs (4, 10, 47). Recently, Burkhardt *et al.* (10) hypothesized that CAIs and this cryptic refractory dust originated both from an inclusion-like chondritic (IC) reservoir, the isotopic composition of which is similar to that of CAIs but the chemical composition of which is similar to bulk chondrites. Mixing of IC reservoir material with material from the NC reservoir would successfully explain the formation of the CC reservoir, and the two would become isolated from one another after the formation of Jupiter (10, 48).

In the framework presented above, the nucleosynthetic processes controlling the bulk composition of CAIs would also control the isotopic difference between CC and NC materials, up to and including planetary-sized bodies. The limited available Sr data obtained from step-leaching experiments of carbonaceous chondrites (6, 7, 10) support this hypothesis. In the studied samples (Ivuna CI chondrite, Murchison CM chondrite, and Tagish Lake C2-ungrouped chondrite), phases digested in dilute acetic acid and low molarity (<5 M) nitric acid at room temperature contain >90% of the total Sr of the meteorite and have positive $\mu^{84}Sr$ values (+45 to +69), consistent with a *p*-nuclide origin of these anomalies. In contrast, the refractory components digested in later leaching steps extend to very negative $\mu^{84}Sr$ values (Ivuna: -3240 ± 120; Murchison: -4741 ± 70; Tagish Lake: -3427 ± 17). The influence of these refractory components is consistent with the presence of SiC grains and variable *s*-process contributions to these bulk CC meteorites, as observed for other elements (e.g., Mo) (49). Yet, these unambiguous *s*-process signatures only result in moderate decreases in the bulk isotopic anomalies of the meteorites measured ($\mu^{84}Sr = -17$ in Ivuna, -17 to 27 in Murchison, and -33 in Tagish Lake), which supports the idea that the positive ^{84}Sr anomalies in bulk CC materials are mainly controlled by materials with a *p*-nuclide excess (through addition of CAI and CAI-like components).

There is a clear isotopic difference between the refractory components isolated from fg-CAIs (whose composition is thought to represent the average early infalling molecular cloud material: the IC reservoir) and bulk CC meteorites (thought to represent a mixture

of IC and NC materials). This observation supports proposals of a heterogeneous distribution of presolar grains in the presolar molecular cloud, as a result of changes in the composition of the material infalling on the protosolar nebula (*45*, *48*, *50*). The extreme ^{84}Sr excesses reported here in fg-CAIs also deepen the gap between the "normal" and FUN CAIs, which display large negative ^{84}Sr anomalies. The bulk FUN CAIs EK-1-4-1 and C1 (*5*) are characterized by negative μ^{84}Sr values of about −3200 and −700, respectively, and the leached FUN CAI CMS-1 (*32*) extends to about −420 and −560. These results suggest that the main carriers of ^{84}Sr anomalies in fg-CAIs are fundamentally different from those in FUN Allende CAIs.

Implications for Rb-Sr chronologies of the early solar system

Our data have important implications for the chronology of volatile element depletion in planetary materials (*12*, *17*). Taken at face value, the differences between the ^{87}Sr/^{86}Sr initial ratios of CAIs and differentiated NC meteorites, such as eucrites and angrites, yield model ages for these meteoritic parent bodies that are equivalent to (*17*), or longer than (*24*), their core formation and accretion time scales as derived from Hf-W and Mn-Cr systematics (e.g., (*51*)). This feature was considered by Halliday and Porcelli (*12*) to represent formation of the eucrite/angrite parent bodies with a solar or higher than solar Rb/Sr ratio, followed by a period of rapid ingrowth of ^{87}Sr, before large-scale volatile depletion to explain the very alkali-poor nature of these meteorites (present Rb/Sr ~1 to 2 orders of magnitude lower than the solar value).

As an alternative, Moynier *et al.* (*13*) and Hans *et al.* (*17*) argued that the indistinguishable initial ^{87}Sr/^{86}Sr for eucrites and angrites [that is, BABI (basaltic achondrite best initial)] versus the lower value for CAIs reflected an anomaly in the normalizing ^{86}Sr/^{88}Sr ratio and that when "corrected for" removed the ^{84}Sr anomaly and made the Gray *et al.* (*24*) USNM 3898 value for initial ^{87}Sr/^{86}Sr match that of eucrites and angrites. Settling this debate therefore boils down to identifying which nucleosynthetic process is responsible for the apparent ^{84}Sr anomalies of CAIs relative to the NC planetary materials (angrites and eucrites). The magnitudes and direction of the ^{84}Sr offsets we measured in leach fractions L4 and L5 show unequivocally that the anomalies must lie in ^{84}Sr. This conclusion renders the proposal of Hans *et al.* (*17*) untenable and agrees with previous work (*22*, *23*, *32*, *52*) that pointed out that the Allende FUN inclusions similarly show diverse ^{84}Sr variations yet coherent initial ^{87}Sr/^{86}Sr initial values, closely comparable to the canonical USNM 3898 CAI (*24*). In our results, the initial ^{87}Sr/^{86}Sr value of 0.698784 ± 0.000076 yielded by the isochron from the step L4 aliquots (i.e., the closest our step-leaching protocol came to isolating the primary condensate mineralogy in the CAIs) is indistinguishable, within error, from those derived for ALL [0.69877 ± 0.00004 (*24*) and 0.698808 ± 0.000020 (*21*)]. Thus, if there are any variations in the *r*- versus *s*-process isotopic balance of ^{88}Sr (within the limits of error of the measurements we make; Fig. 5), these are concealed within the variability of the bulk data. Our results thus reinstate the distinction in initial ^{87}Sr/^{86}Sr values between the inner solar system–differentiated materials (NC reservoir) represented by eucrites and angrites (*11*, *53*) on the one hand, and CAIs and CC meteorites on the other hand, and suggest that this difference holds a chronological significance. Translating this distinction into a time scale is, however, hindered by our lack of knowledge of the initial Rb/Sr ratios of the angrite and eucrite parent bodies. Although beyond the scope of this paper, careful re-evaluation of this issue will be needed to place robust constraints on the time

scales of volatile depletion in the early solar system based on Rb-Sr systematics.

MATERIALS AND METHODS

Samples

Nine fg-CAIs from Allende were investigated in this study. Table 1 gives the sample numbers as used here, plus the catalog numbers in the American Museum of Natural History database, and sample masses taken for both the step-leaching experiments and bulk analysis. The samples were initially identified on the basis of their texture (fine-grained), color (from white/gray to purple, with most being pink due to FeO in spinel), and irregular shapes. They were excised from cut slabs of Allende and crushed in a class 1000 laboratory at the Massachusetts Institute of Technology (McGee lab), using the methods described in Tissot *et al.* (*54*). A small chip of each CAI was extracted using cleaned stainless steel dental tools (Hu-Friedy: see below for the metal composition), under a stereoscopic zoom microscope, and mounted in epoxy for microbeam investigation to confirm the classification of the samples as fg-CAIs, based on their typical textures, compositions, and mineralogy [e.g., (*25*, *54*)] For each CAI, secondary electron and back-scattered electron images, along with mineral identifications, are shown in figs. S1 to S9.

In most samples, primary mineral phases were found to be spinel (predominantly), perovskite (minor occurrences), and sometimes melilite. Two samples (*Erik* and *Logan*) showed, respectively, hibonite and pyroxene, as another major phase. These features are consistent with the typical mineralogy of fg-CAIs (*55*, *56*). As is common for fg-CAIs from Allende, all samples have experienced significant alteration as evidenced by the abundance of secondary phases such as nepheline, sodalite, grossular, anorthite, and hedenbergite, as well as the presence of clinopyroxene rims around spinel (*57*). Forsterite was found in most samples, mostly concentrated in the rim of the CAIs, similar to the outermost zone C in inclusions described by Hashimoto and Grossman (*57*), and as individual occurrences inside some of the samples. Trace occurrences of Fe-Ni metal as well as iron and/or titanium oxides (i.e., ilmenite and magnetite) were also observed.

Sample preparation and step leaching

The powdered CAIs were weighed out into preweighed, clean conical-bottomed perfluoroalkoxy alkane (PFA) Savillex beakers, and step leaching was carried out using acids of different concentration while varying the temperature and duration of treatment. The entire leaching process and subsequent aliquoting, column chemistry, and dilution procedures were performed at VUW in an ultraclean environment using high-purity distilled acids and water produced by two-time subboiling distillation in Teflon stills (TD reagents; see information on procedural blanks below). Step leaching (L) dissolution used the following sequence:

1) L1: 0.5 M CH_3CO_2H (acetic acid), 1 day, 20°C, shaken up by hand every few hours;

2) L2: 0.5 M HNO_3, 3 days, 20°C, shaken up by hand two to three times a day;

3) L3: 6 M HCl, 1 day, 120°C, sonicated for 15 min at the beginning;

4) L4: 14 M HF, 9 M HNO_3, 1 day, 120°C, sonicated for 15 min at the beginning;

5) L5 (final digest): 14 M HF, 9 M HNO_3, 3 days, 220°C, high pressure Parr bomb digest.

This protocol broadly follows previous studies [e.g., (58)]: L1 should only mobilize the soluble alteration phases; L2 would digest more of the alteration phases; L3 would presumably start digesting oxide, silicate, and metal; L4 would digest most minerals except for the most refractory phases; and L5 is a full digestion of the residue in a pressurized vessel. The aliquot fractions were labeled by leach step (L1 to L5) and sample name (_name). After each leaching step, the beakers were secured within custom-made holders and centrifuged at 5000 rpm (5 min). The supernatant liquid was pipetted off to a separate clean beaker, taking care not to disturb the sediment pellet in the conical tip of the beaker. TD water (1 to 2 ml) was then added to the beaker, and the sediment pellet was resuspended via shaking and several minutes of sonication. This process was repeated three times to ensure full leachate solution recovery. The beaker containing the pellet was then returned to a hotplate and taken to dryness at 120°C. After re-equilibration to ambient temperature, the beakers containing the pellets were weighed again, and the difference between initial weight at the start of the leach step and the postleaching weight was taken to represent the amount of sample digested at each leach step (allowing calculation of trace elements concentration in the mass fraction of the sample digested in each step).

Leachate solutions produced in steps L1 to L4 were taken to dryness, treated with aqua regia (3:1 HCl/HNO$_3$), dried once more, and then redissolved in 2 ml of 9 M HNO$_3$. The *Logan* CAI was completely dissolved by the end of the L4 stage, and no residues were visible under a binocular microscope. For all other samples, the remaining grains in the final residue (L5) were removed from the conical vial, weighed using an ultra-microbalance, transferred into Parrish-type capsules, and digested in HNO$_3$-HF (1:5) over 3 days using Parr bomb high pressure digestion vessels in an oven at 220°C. After the final digestion, L5 samples were rinsed out of their capsules into conventional Savillex vials, and complete dissolution following the addition of 6 M HCl was verified using a binocular microscope. The samples were taken to dryness and lastly taken up in 2 ml of 9 M HNO$_3$.

For all sample solutions (L1 to L5) in 9 M HNO$_3$, a 5 to 10% aliquot was taken and diluted appropriately for trace element analysis using a Thermo Fisher Element 2 sector field ICP-MS instrument, although for this paper only, the Rb, Sr, and REE contents are used (the full dataset will be presented elsewhere). Calibration curves (i.e., concentration versus count rates) for each element were generated using a range of USGS rock standards (BHVO-2, BCR-2, and AGV-2) as well as synthetic standards prepared gravimetrically from commercially available, certified, single-element standards. The range in standards was chosen to bracket the calculated ranges in concentrations of the diluted leach and residue fractions. Count times were extended for Rb and Sr to reduce the uncertainty on the parent-daughter ratio determinations, and instrumental drift was monitored and corrected for using repeated analysis of a standard measured for every two unknowns. Blank subtraction for the trace element data was carried out using the measured concentrations in a total procedure blank that had been produced under the same conditions as for sample processing (see below).

For the Sr isotope work, the remaining sample was further split at the 9 M HNO$_3$ stage into two fractions. One half was spiked with the VUW ^{84}Sr-^{87}Sr double spike (DS aliquot) (4) for stable isotope determination and the other half left unspiked (natural aliquot) for conventional, internally normalized analysis. Purification of Sr from the sample matrix was performed by extraction chromatography using Sr-spec resin by sorption onto the resin and matrix elution

using 9 M HNO$_3$ and then back extraction of the Sr in 0.05 M HNO$_3$. Natural and DS aliquots were processed separately using labware specifically designated for spiked and natural samples. The techniques for this part of the study are identical to those detailed in the supplementary materials for Charlier *et al.* (8).

Aliquots of the bulk powder from each CAI were also investigated. These were first weighed using an ultra-microbalance and then transferred into Savillex vials for initial HF-HNO$_3$ digestion under low pressure at 130°C. Any remaining residues were then transferred to Parrish-type capsules and digested in HNO$_3$-HF (1:5) over 3 days at 220°C in a high-pressure Parr bomb. After complete digestion, total bulk CAI samples were processed using the same column protocols as those for the leach fractions.

Because of the susceptibility of the exceedingly small load sizes encountered in L5, great care was taken to eliminate all possibility of contamination with materials that could influence the ^{84}Sr abundances. Spike contamination can be eliminated as a possible influence on the data for the following reasons.

1) The step leaching process was carried out on the samples before the isotopic spike material was used in the laboratory. The samples, in solution in their factory new beakers, had a fraction aliquoted for ICP-MS trace element analysis, and a second aliquot was taken and processed through column chemistry for natural ratio analysis (which is what yielded the values used by internal normalization for the µ^{84}Sr anomalies obtained for this study). Only then did the remaining material have the spike added to it. The first two steps, in all cases, were undertaken before the spike was used in the clean handling facilities (which had not previously seen the use of any enriched Sr isotopic spike materials).

2) All materials used for spiked analyses were kept entirely separate: independent collections of Teflon beakers for natural and double-spiked samples, separate filaments, and working spaces with only one operator active at any stage for this work. Cleaning protocols associated with laboratory items and consumables for spike versus natural materials involved entirely separate vessels and reagents.

3) In addition to the standards run during data collection for this study, we have also subsequently measured ~1-ng samples of natural standard BCR-2 processed using the same protocols as our CAI samples in the VUW laboratories but after the Sr spike material had been opened and used extensively in the laboratory. The NBS-987 data on picogram-level loads (table S2 and fig. S11) serve to demonstrate that any possible contamination could not have occurred at the loading (VUW) or analysis (Bremen) stages, as the 1- to 2-ng-level BCR-2 data (i.e., comparable sample loads to the L4, L5 fractions were analyzed in this study) show no detectable contamination (table S3 and fig. S11).

Mass spectrometry

Strontium isotopic compositions were measured using two TIMS instruments. A Thermo-Finnigan Triton at VUW, equipped with nine Faraday collectors connected to 10^{11}-ohm feedback resistor amplifiers, and a Thermo Scientific Triton XT at the Thermo Fisher Scientific factory in Bremen, Germany, equipped with a switchable selection of both 10^{11}- and 10^{13}-ohm amplifiers. Gain calibration was performed before each day of analysis, and the interchannel gain stability of the 10^{11}- and 10^{13}-ohm amplifier equipped instruments was better than 25 ppm/24 hours and 10 ppm/24 hours (2 SD), respectively.

The VUW instrument was used for the analysis of the fractions L1 to L3, where the Sr load was >100 ng in all cases. Analyses consisted

of 540 cycles (16-s integrations) measured statically with amplifier rotation, a 1-min baseline measurement, and a prebaseline wait time of 20 s after each rotation (4, 8). The Bremen instrument, with the improved signal-to-noise ratio afforded by the 10^{13}-ohm amplifiers (30), was used for analysis of the smaller load sizes produced in leach fractions L4 and final digest L5. This instrument was configured with the 10^{13}-ohm amplifiers connected to cups L1, C, H1, and H2 for measurement of masses ^{84}Sr, ^{85}Rb, ^{86}Sr, and ^{87}Sr, respectively, using cup H3 to collect ^{88}Sr using a 10^{11}-ohm amplifier. No amplifier rotation was performed, and a single 20-min baseline was measured with the analyzer valve closed during sample warm-up. After tuning and instrument optimization, measurements were made in static mode, using 4.194-s integration time, and collecting up to 400 cycles, or until the sample was completely exhausted. After each block of 40 cycles, the signal was checked and the evaporation filament current adjusted by the software so that the signal remained within 80 and 120% of the intensity measured at the start of the run. The bulk CAI samples were run later on the VUW instrument after upgrading with four 10^{13}-ohm amplifiers, one of which was used to measure mass 84 during those runs (other masses measured on 10^{11}-ohm amplifiers).

For all measurements, any ^{87}Rb interferences at mass 87 were corrected for using the beam intensity measured at ^{85}Rb and assuming $^{87}Rb/^{85}Rb = 0.385707$ (59). In all runs, the raw ^{87}Rb contribution to the ^{87}Sr signal never exceeded a few microvolts and was observed to decay rapidly before the start of analysis. Natural (unspiked) runs were corrected for instrumental fractionation using the exponential law to $^{86}Sr/^{88}Sr = 0.1194$. Double spike measurements and subsequent data reduction were carried out using the methods detailed in Charlier et al. (4, 8). All samples were loaded on outgassed zone-refined single Re filaments, and a Ta_2F_5 activator (60) was used to increase ionization efficiency. Natural and spiked measurements were made on separate sample wheels with a clean ion-source extraction plate for each wheel change. Loading of filaments was carried out at VUW using identical techniques throughout and the same batch of Re wire. Care was taken to retain consistency in both the nature and quality of sample loading with the intention of keeping the total procedural blank as uniform as possible for all analyses. Filaments loaded at VUW were sealed within a clean environment and carefully transported to Bremen for analysis.

Notations

Following the convention for the reporting of ^{84}Sr anomalies used in other studies, we use the $\mu^{84}Sr$ notation (i.e., parts per 10^6 deviation of the $^{84}Sr/^{86}Sr$, internally normalized to $^{86}Sr/^{88}Sr = 0.1194$, from the average value of the standard)

$$\mu^{84}Sr = \left[\frac{(^{84}Sr/^{86}Sr)_{samp}}{(^{84}Sr/^{86}Sr)_{NBS-987\ ave}} - 1 \right] \times 10^6$$

Stable Sr data derived from the double-spike natural measurements are presented in the delta notation (in per mil) relative to our NBS-987 standard

$$\delta^{84/86}Sr(\permil) = \left[\frac{(^{84}Sr/^{86}Sr)_{samp}}{(^{84}Sr/^{86}Sr)_{NBS-987}} - 1 \right] \times 10^3$$

$$\delta^{88/86}Sr(\permil) = \left[\frac{(^{88}Sr/^{86}Sr)_{samp}}{(^{88}Sr/^{86}Sr)_{NBS-987}} - 1 \right] \times 10^3$$

All of the fractionation-corrected $^{87}Sr/^{86}Sr$ data have been renormalized to NBS-987 = 0.710250.

Data precision and accuracy

The NBS-987 strontium standard was run at various load sizes to assess the reproducibility for the load sizes measured on each instrument. The details of these measurements are given in table S2, and the standard reproducibility was summarized in Results. For the large loads encountered in L1 to L3, internally normalized measurements of nine ~1000-ng loads of the standard were carried out over the period of analysis on the VUW instrument. Given that the double-spike data involve two independent mass spectrometric measurements, eight NBS-987 loads optimally spiked with the VUW ^{84}Sr-^{87}Sr double spike were measured during the same period, and the data were reduced against each of the natural NBS-987 runs to yield 72 possible permutations to calculate the external reproducibility. For the Bremen instrument, 10 individual measurements of 1-ng, 500-pg, and 50-pg NBS-987 loads were carried out. One sample of the 50-pg loading was discarded because of an ion yield of <0.1%. Average Sr ion yields (data were only measured for acquisition where signals were higher than 10 mV on ^{88}Sr) were 1.5, 1.8, and 1.5%, and the average ^{84}Sr signals were 5.5, 3.2, and 0.3 μV, for, respectively, the 1-ng, 500-pg, and 50-pg Sr loadings. The external precisions for individual analyses (table S2) are within a factor of 1.5 of the average internal precisions as defined by the counting statistics. For the stable strontium measurements, an overall external reproducibility for $\delta^{84/86}Sr$ and $\delta^{88/86}Sr$ for small load sizes was determined for the 1-ng loads where the 10 analyses of unspiked, natural NBS-987 were deconvolved against nine optimally spiked 1-ng aliquots.

As an additional demonstration of data consistency between the VUW and Bremen instruments, both the natural and spiked aliquots of two samples (L3_Jean and L3_Logan) were measured first at VUW then later at Bremen (fig. S14) and yielded identical results (within uncertainty). These samples were chosen on the basis that enough Sr remained on the filament for two measurements since the measured isotopic composition for the natural aliquots had not yet fractionated through the $^{86}Sr/^{88}Sr = 0.1194$ value assumed for fractionation correction.

To check for the integrity and consistency of isotopic data from the gravimetric recombined leach fractions, we carried out analysis of total digests of the remaining fractions of bulk powder from the individual CAIs. In addition, these analyses served to constrain the magnitude of any possible spike contribution to any ^{84}Sr values in the leachate samples from the natural runs. The $\mu^{84}Sr$ values from the bulk samples are presented in table S4 and plotted in Fig. 2 and show good agreement with the reconstituted L1 to L5 compositions. In particular, Jean, which has the largest $\mu^{84}Sr$ value, shows a match within error for reconstituted L1 to L5 and the bulk sample, and both of these are distinct from the L1 to L3 data (Fig. 2).

Possible sources of inaccuracies
Blank contributions

An identical conical beaker to that used in the step-leaching procedure, but containing no sample, was manipulated in the same way as the sample beakers and the subsequent sample-free supernatants passed through identical column chemistry and aliquoting for trace element analysis. The blank amount for each leach step was calculated via isotope dilution (ID) using an ^{84}Sr single spike, which was diluted from an "as-supplied" IRMM-635 1 M HNO_3 stock solution

and calibrated for concentration against a gravimetric solution of NBS-987. ID mass spectrometric measurements were made at different times to those of the unknowns and used an entirely separate suite of labware and filament components to circumvent any possibility of cross-contamination with ^{84}Sr.

To blank-correct the isotopic data, both the blank amount and its isotopic composition must be known. From past work in the VUW laboratory, the largest contributor to the total procedural blank (TPB) has been found to derive chiefly from the Sr-spec resin used for separation. The wash fractions from the resin cleaning procedure were thus collected (60), and their isotope composition was precisely measured, yielding a value of ^{87}Sr/^{86}Sr = 0.709866 ± 0.000003 (2 SD; normalized to NBS-987 ^{87}Sr/^{86}Sr = 0.710250) as a best estimate for the TPB composition for correction of radiogenic data. The internally normalized ^{84}Sr/^{86}Sr (μ^{84}Sr) data were blank-corrected using the measured ^{84}Sr/^{86}Sr value for NBS-987 obtained from the respective instrument. Double spike data were corrected for blank assuming "average BSE" values of 0.3 and −0.3‰ for $\delta^{88/86}$Sr and $\delta^{84/86}$Sr, respectively (8). The TPBs were remarkably consistent at 55 ± 13 pg (2 SD) total strontium for all leach steps. In the case of L1 to L3, the TPB never exceeded 0.14% of the Sr present. For steps L4 and L5, TPB contributions ranged from 0.23 to 5.30% and 0.082 to 24.82% of the Sr present in each sample aliquot, respectively (table S4). The two TPBs measured for the bulk CAI digests gave an average of 66.2 pg, representing a maximum blank contribution of 0.11% in these analyses. To ensure consistency, blank corrections were made to the isotopic data for the bulk analyses and all leach fractions, regardless of total strontium content.

Tests for coherent fraction behavior of processed samples

To test for the possibility that separation of Sr from a matrix dominated by Ca and Al could lead to anomalous fractionation behavior during ionization from the filament, some "synthetic CAI" solutions were prepared. These solutions were made from ICP-MS single-element standards containing an identical mixture of the major elements (Mg, Al, Ca, and Fe) to mimic the composition of the final leachates determined for the three most extreme μ^{84}Sr-bearing samples (L5_*Hank*, L5_*Ororo* and L5_*Peter*; μ^{84}Sr = +80655, +11599, and + 5225, respectively). Ten nanograms of NBS-987 Sr was added to each of these solutions, which were then subjected to the same Sr-spec column separation as that used for the unknowns throughout this study. Natural logs of the measured ratios of the separated Sr were used to produce regression lines in three-isotope ^{87}Sr denominator space, from which a slope could be determined using a best-fit York-type regression to the block average data. The slopes of the lines for each synthetic solution were then compared and found to agree, within uncertainty, with those expected for theoretical exponential law fractionation (table S5). This demonstrates that the highly anomalous data for residues measured in L4 and L5 are not an artifact of nonexponential law ionization behavior during TIMS analysis and that the use of internal normalization using the exponential law is justified.

Tests on the extraction tools used for sampling CAIs

The CAIs were extracted from their host meteorite using cleaned stainless steel and nickel-cobalt-molybdenum alloy dental tools [after (54)]. To test for possible contamination from these tools, their Sr contents and isotopic compositions were determined. Tool fragments were removed using a diamond saw blade, lubricated, and cooled with water. Each tool was cut half way through then covered with a laboratory tissue and snapped by hand against a hard surface.

The fragments of the four tools (DT-1 to DT-4) were cleaned repeatedly using Milli-Q H$_2$O and ultrapure ethanol in an ultrasonic bath and then dried in an oven. They were then weighed and dissolved using increasingly aggressive acids, culminating in full digestion in aqua regia for the stainless-steel tools (DT-1, DT-3, and DT-4). DT-2 (NiCoMo alloy), however, was not fully dissolved even after protracted acid digestion at elevated temperatures. This fragment was reweighed, and the difference between the initial and incompletely digested fragment mass was taken as the sample weight in solution. All solutions were equilibrated in 9 M HNO$_3$ before aliquoting and column chemistry. A ca. 10% aliquot was mixed gravimetrically with the same ^{84}Sr spike as that used for TPBs to determine the Sr concentration via ID, and the remainder left unspiked for isotopic analysis. Both aliquots were processed separately through columns using the same methods as for the natural samples. Sr concentrations and isotopic compositions in dental tool materials are given in table S6.

Given that the tools were not weighed before and after the CAI sampling, their exact contribution to the Sr budget of the sample is uncertain, yet, as shown below, significant contamination can be ruled out. For all samples, full digestion after the final bomb digest was ascertained by careful inspection of the liquid under a binocular microscope after removal from the bomb. No discernable particulate matter was observed in any samples after the final digestion (L5). Given the resistance to acid digestion described above (particularly for DT-2), any metal swarf generated from the tools from abrasion against the sample would have been unlikely to be dissolved in the first three leach steps and may possibly have survived through to the final digest where its effect on the isotopic composition of the sample would have had the largest influence.

To test the possible influence of the dental tools on the isotopic composition of the samples, we examined an extreme worst-case scenario of 1 mg of dental tool being present in the final digestion. This figure is based on observations that the tools were visually unaffected by the abrasion process, and a loss of 1 mg or more of material would have been obvious from visual inspection. In terms of the ^{84}Sr influence, we consider CAI sample L5_*Hank*, which contained the smallest Sr amount (0.372 ng) but the most extreme μ^{84}Sr (+80,655). Taking DT-2 as the tool likely to exert the largest effect on the Sr budget of the sample (due to its high Sr content; 215.6 parts per billion), 1 mg of this tool represents 0.2156 ng of Sr. For L5_*Hank*, this would correspond to a "blank" contribution of ~58% and yield a μ^{84}Sr value blank-corrected upward to +192,184 (on account of the μ^{84}Sr of the dental tools having essentially normal μ^{84}Sr). In contrast, correction of the measured ^{87}Sr/^{86}Sr would be revised downward from 0.704163 to a very unradiogenic value of 0.697339. In this scenario, the presence of dental tool material in the analysis would serve to reduce the measured μ^{84}Sr, not increase it, but raises the possibility that the ^{87}Sr/^{86}Sr might be shifted to apparently more radiogenic measured values if this dental tool material were present.

In terms of ^{87}Sr, to test whether the more radiogenic ^{87}Sr/^{86}Sr values encountered for some samples (in particular, in the L5 step) were affected by contamination from dental tool material, we consider the possible effects of tool material addition to L5_*Scott*. This sample contained 58.2-ng Sr in the final digest and has the most radiogenic measured ^{87}Sr/^{86}Sr of all the final leach fractions (^{87}Sr/^{86}Sr = 0.706701). Again, assuming the worst-case scenario of 1 mg of tool contamination from DT-2, the blank contribution in this situation would be only 0.37%. This would result in negligible shifts in the

corrected ratios (μ^{84}Sr, +854 revised upward to +857; ^{87}Sr/^{86}Sr, 0.706701 revised downward to 0.706692). On this basis, the values measured for CAI 9 and others with extreme values in the L5 step must therefore represent the primary isotopic compositions of these samples.

The same mass balance considerations using the other three sampling tools yield the same conclusions and demonstrate that the observed highly anomalous μ^{84}Sr values encountered in steps L4 and L5 cannot be attributed to any admixture of material from the sampling process, since none of the dental tools have an elevated μ^{84}Sr. Similarly, the measured, highly radiogenic ^{87}Sr/^{86}Sr values in steps L4 and L5 cannot be attributed to material derived from any of the dental tools used and must be of primary origin, particularly those measured in the L5 step. Last, the influence on the measured Sr isotopic compositions of any dental tool material contribution at an earlier stage in the leaching process (L1 to L3) would have been trivially small on account of the much higher Sr contents encountered in these preceding leach fractions.

Geochemical insights into the nature of the ^{84}Sr carrier

In theory, the geochemical signatures of the successive leachates could shed light on the nature of these carrier phases. As major and trace elements were measured on the leachate solutions, we attempted to place constraints on the nature of the carrier using these data. The most informative cross-plots of major and trace element atomic ratios in the leachates are shown in fig. S13. Although the data clearly indicate which of the major phases is being digested in which step (i.e., mixing arrays in between well-defined poles), they do not, however, allow us to pin down the nature of the carriers. This is evident when looking at the third and fourth panels (in which the data for L5 are shown). The chemical composition of the leachate is overwhelmed by those of the major phases, and the L5 leachates define mixing arrays between a spinel pole and an Al-rich diopside pole. This is consistent with a very low abundance of nucleosynthetic anomaly carriers with extremely high ^{84}Sr excess, as observed in L5 in the *Hank* CAI. Establishing the nature of the *p*-process carriers will therefore require additional work and the physical isolation, imaging, and isotopic analysis of the carrier. These steps are beyond the scope of the present study.

SUPPLEMENTARY MATERIALS

Supplementary material for this article is available at http://advances.sciencemag.org/cgi/content/full/7/28/eabf6222/DC1

REFERENCES AND NOTES

1. Y. Amelin, A. Kaltenbach, T. Iizuka, C. H. Stirling, T. R. Ireland, M. Petaev, S. B. Jacobsen, U–Pb chronology of the Solar System's oldest solids with variable ^{238}U/^{235}U. *Earth Planet. Sci. Lett.* **300**, 343–350 (2010).
2. J. N. Connelly, M. Bizzarro, A. N. Krot, Å. Nordlund, D. Wielandt, M. A. Ivanova, The absolute chronology and thermal processing of solids in the solar protoplanetary disk. *Science* **338**, 651–655 (2012).
3. P. J. Patchett, Sr isotopic fractionation in Ca–Al inclusions from the Allende meteorite. *Nature* **283**, 438–441 (1980).
4. B. L. A. Charlier, F. L. H. Tissot, N. Dauphas, C. J. N. Wilson, Nucleosynthetic, radiogenic and stable strontium isotopic variations in fine- and coarse-grained refractory inclusions from Allende. *Geochim. Cosmochim. Acta* **265**, 413–430 (2019).
5. D. A. Papanastassiou, G. J. Wasserburg, Strontium isotopic anomalies in the Allende meteorite. *Geophys. Res. Lett.* **5**, 595–598 (1978).
6. C. Paton, M. Schiller, M. Bizzarro, Identification of an ^{84}Sr-depleted carrier in primitive meteorites and implications for thermal processing in the solar protoplanetary disk. *Astrophys. J. Lett.* **763**, L40 (2013).
7. T. Yokoyama, Y. Fukami, W. Okui, N. Ito, H. Yamazaki, Nucleosynthetic strontium isotope anomalies in carbonaceous chondrites. *Earth Planet. Sci. Lett.* **416**, 46–55 (2015).
8. B. L. A. Charlier, I. J. Parkinson, K. W. Burton, M. M. Grady, C. J. N. Wilson, E. G. C. Smith, Stable strontium isotopic heterogeneity in the solar system from double-spike data. *Geochem. Perspect. Lett.* **4**, 35–40 (2017).
9. K. Myojo, T. Yokoyama, S. Okabayashi, S. Wakaki, N. Sugiura, H. Iwamori, The origin and evolution of nucleosynthetic Sr isotope variability in calcium and aluminium-rich refractory inclusions. *Astrophys. J.* **853**, 48 (2018).
10. C. Burkhardt, N. Dauphas, U. Hans, B. Bourdon, T. Kleine, Elemental and isotopic variability in solar system materials by mixing and processing of primordial disk reservoirs. *Geochim. Cosmochim. Acta* **261**, 145–170 (2019).
11. D. A. Papanastassiou, G. J. Wasserburg, Initial strontium isotopic abundances and the resolution of small time differences in the formation of planetary objects. *Earth Planet. Sci. Lett.* **5**, 361–376 (1969).
12. A. N. Halliday, D. Porcelli, In search of lost planets – the paleocosmochemistry of the inner solar system. *Earth Planet. Sci. Lett.* **192**, 545–559 (2001).
13. F. Moynier, J. M. D. Day, W. Okui, T. Yokoyama, A. Bouvier, R. J. Walker, F. A. Podosek, Planetary-scale strontium isotopic heterogeneity and the age of volatile depletion of early solar system materials. *Astrophys. J.* **758**, 45 (2012).
14. E. D. Young, A. Galy, H. Nagahara, Kinetic and equilibrium mass-dependent isotope fractionation laws in nature and their geochemical and cosmochemical significance. *Geochim. Cosmochim. Acta* **66**, 1095–1104 (2002).
15. F. Moynier, A. Agranier, D. C. Hezel, A. Bouvier, Sr stable isotope composition of Earth, the Moon, Mars, Vesta and meteorites. *Earth Planet. Sci. Lett.* **300**, 359–366 (2010).
16. B. L. A. Charlier, G. M. Nowell, I. J. Parkinson, S. P. Kelley, D. G. Pearson, K. W. Burton, High temperature strontium stable isotope behaviour in the early solar system and planetary bodies. *Earth Planet. Sci. Lett.* **329-330**, 31–40 (2012).
17. U. Hans, T. Kleine, B. Bourdon, Rb–Sr chronology of volatile depletion in differentiated protoplanets: BABI, ADOR and ALL revisited. *Earth Planet. Sci. Lett.* **374**, 204–214 (2013).
18. G. A. Brennecka, L. E. Borg, M. Wadhwa, Evidence for supernova injection into the solar nebula and the decoupling of *r*-process nucleosynthesis. *Proc. Natl. Acad. Sci. U.S.A.* **110**, 17241–17246 (2013).
19. Q. R. Shollenberger, L. E. Borg, J. Render, S. Ebert, A. Bischoff, S. S. Russell, G. A. Brennecka, Isotopic coherence of refractory inclusions from CV and CK meteorites: Evidence from multiple isotope systems. *Geochim. Cosmochim. Acta* **228**, 62–80 (2018).
20. K. Lodders, Solar system abundances and condensation temperatures of the elements. *Astrophys. J.* **591**, 1220–1247 (2003).
21. F. A. Podosek, E. K. Zinner, G. J. MacPherson, L. L. Lundberg, J. C. Brannon, A. J. Fahey, Correlated study of initial ^{87}Sr/^{86}Sr and Al-Mg isotopic systematics and petrologic properties in a suite of refractory inclusions from the Allende meteorite. *Geochim. Cosmochim. Acta* **55**, 1083–1110 (1991).
22. D. A. Papanastassiou, Initial ^{87}Sr/^{86}Sr chronology; a journey through 4.5 decades, in *Proceedings of the 46th Lunar Planetary Science Conference*, (2015), 2243.
23. D. A. Papanastassiou, J. H. Chen, Initial ^{87}Sr/^{86}Sr chronology in the solar system, in *Proceedings of the 47th Lunar Planetary Science Conference*, (2016), 2650.
24. C. M. Gray, D. A. Papanastassiou, G. J. Wasserburg, The identification of early condensates from the solar nebula. *Icarus* **20**, 213–239 (1973).
25. L. Grossman, R. M. Fruland, D. S. McKay, Scanning electron microscopy of a pink inclusion from the Allende meteorite. *Geophys. Res. Lett.* **2**, 37–40 (1975).
26. L. Grossman, Condensation in the primitive solar nebula. *Geochim. Cosmochim. Acta* **36**, 597–619 (1972).
27. S. Yoneda, L. Grossman, Condensation of CaO–MgO–Al$_2$O$_3$–SiO$_2$ liquids from cosmic gases. *Geochim. Cosmochim. Acta* **59**, 3413–3444 (1995).
28. D. S. Ebel, Condensation of rocky material in astrophysical environments, in *Meteorites and the Early Solar System II*, D. S. Lauretta, H. Y. McSween Jr., Eds. (University of Arizona Press, 2006), pp. 253–277.
29. J. Y. Hu, N. Dauphas, F. L. H. Tissot, R. Yokochi, T. J. Ireland, Z. Zhang, A. M. Davis, F. J. Ciesla, L. Grossman, B. L. A. Charlier, M. Roskosz, E. E. Alp, M. Y. Hu, J. Zhao, Heating events in the nascent solar system recorded by rare earth element isotopic fractionation in refractory inclusions. *Sci. Adv.* **7**, eabc2962 (2021).
30. J. M. Koornneef, C. Bouman, J. B. Schwieters, G. R. Davies, Measurement of small ion beams by thermal ionisation mass spectrometry using new 10^{13} Ohm resistors. *Anal. Chim. Acta* **819**, 49–55 (2014).
31. G. J. MacPherson, C. Defouilloy, N. T. Kita, High-precision Al–Mg isotopic systematics in USNM 3898–The benchmark "ALL" for initial ^{87}Sr/^{86}Sr in the earliest Solar System. *Earth Planet. Sci. Lett.* **491**, 238–243 (2018).
32. Y. Amelin, C. D. Williams, M. Wadhwa, U-Th-Pb and Rb-Sr systematics of Allende FUN CAI CMS-1, in *Proceedings of the 46th Lunar Planetary Science Conference* (2015), 2355.
33. G. R. Huss, The survival of presolar grains in solar system bodies. *AIP Conf. Proc.* **402**, 721–748 (1997).

34. G. R. Huss, R. S. Lewis, Presolar diamond, SiC, and graphite in primitive chondrites: Abundances as a function of meteorite class and petrologic type. *Geochim. Cosmochim. Acta* **59**, 115–160 (1995).

35. E. K. Zinner, Presolar grains, in *Treatise on Geochemistry, Vol. 1, Meteorites, Comets, and Planets*, H. D. Holland, K. K. Turekian, A. M. Davis, Eds. (Elsevier, 2003), pp. 1–33.

36. O. Pravdivtseva, F. L. H. Tissot, N. Dauphas, S. Amari, Evidence of presolar SiC in the Allende Curious Marie calcium-aluminium-rich inclusion. *Nat. Astron.* **4**, 617–624 (2020).

37. G. K. Nicolussi, M. J. Pellin, R. S. Lewis, A. M. Davis, R. N. Clayton, S. Amari, Strontium isotopic composition in individual circumstellar silicon carbide grains: A record of s-process nucleosynthesis. *Phys. Rev. Lett.* **81**, 3583–3586 (1998).

38. T. Stephan, R. Trappitsch, A. M. Davis, M. J. Pellin, D. Rost, M. R. Savina, M. Jadhav, C. H. Kelly, F. Gyngard, P. Hoppe, N. Dauphas, Strontium and barium isotopes in presolar silicon carbide grains measured with CHILI—Two types of X grains. *Geochim. Cosmochim. Acta* **221**, 109–126 (2018).

39. T. Stephan, R. Trappitsch, P. Hoppe, A. M. Davis, M. J. Pellin, O. S. Pardo, Molybdenum isotopes in presolar silicon carbide grains: Details of s-process nucleosynthesis in parent stars and implications for r-and p-processes. *Astrophys. J.* **877**, 101 (2019).

40. T. Rauscher, N. Dauphas, I. Dillmann, C. Fröhlich, Z. Fülöp, G. Gyürky, Constraining the astrophysical origin of the p-nuclei through nuclear physics and meteoritic data. *Rep. Prog. Phys.* **76**, 066201 (2013).

41. T. Rauscher, A. Heger, R. D. Hoffman, S. E. Woosley, Nucleosynthesis in massive stars with improved nuclear and stellar physics. *Astrophys. J.* **576**, 323–348 (2002).

42. C. Travaglio, F. K. Röpke, R. Gallino, W. Hillebrandt, Type Ia supernovae as sites of the p-process: Two-dimensional models coupled to nucleosynthesis. *Astrophys. J.* **739**, 93 (2011).

43. G. R. Huss, R. S. Lewis, Noble gases in presolar diamonds I: Three distinct components and their implications for diamond origins. *Meteoritics* **29**, 791–810 (1994).

44. G. R. Huss, A. P. Meshik, J. B. Smith, C. M. Hohenberg, Presolar diamond, silicon carbide, and graphite in carbonaceous chondrites: Implications for thermal processing in the solar nebula. *Geochim. Cosmochim. Acta* **67**, 4823–4848 (2003).

45. N. Dauphas, E. A. Schauble, Mass fractionation laws, mass-independent effects, and isotopic anomalies. *Annu. Rev. Earth Planet. Sci.* **44**, 709–783 (2016).

46. P. H. Warren, Stable-isotopic anomalies and the accretionary assemblage of the Earth and Mars: A subordinate role for carbonaceous chondrites. *Earth Planet. Sci. Lett.* **311**, 93–100 (2011).

47. S. Gerber, C. Burkhardt, G. Budde, K. Metzler, T. Kleine, Mixing and transport of dust in the early solar nebula as inferred from titanium isotope variations among chondrules. *Astrophys. J. Lett.* **841**, L17 (2017).

48. J. A. Nanne, F. Nimmo, J. N. Cuzzi, T. Kleine, Origin of the non-carbonaceous–carbonaceous meteorite dichotomy. *Earth Planet. Sci. Lett.* **511**, 44–54 (2019).

49. G. Budde, C. Burkhardt, T. Kleine, Molybdenum isotopic evidence for the late accretion of outer Solar System material to Earth. *Nat. Astron.* **3**, 736–741 (2019).

50. F. C. Pignatale, S. Charnoz, M. Chaussidon, E. Jacquet, Making the planetary material diversity during the early assembling of the solar system. *Astrophys. J. Lett.* **867**, L23 (2018).

51. T. Kleine, U. Hans, A. J. Irving, B. Bourdon, Chronology of the angrite parent body and implications for core formation in protoplanets. *Geochim. Cosmochim. Acta* **84**, 186–203 (2012).

52. Y. Di, Y. Amelin, Heterogeneous nucleosynthetic 84Sr anomalies within and among CAIs, in proceedings of the 2020 Goldschmidt Conference (2020), 21 to 26 June, https://doi.org/10.46427/gold2020.570.

53. G. W. Lugmair, S. J. G. Galer, Age and isotopic relationships among the angrites Lewis Cliff-86010 and Angra dos Reis. *Geochim. Cosmochim. Acta* **56**, 1673–1694 (1992).

54. F. L. H. Tissot, N. Dauphas, L. Grossman, Origin of uranium isotope variations in early solar nebula condensates. *Sci. Adv.* **2**, e1501400 (2016).

55. L. Grossman, R. Ganapathy, Trace elements in the Allende meteorite—II. Fine-grained. Ca-rich inclusions. *Geochim. Cosmochim. Acta* **40**, 967–977 (1976).

56. A. N. Krot, G. J. MacPherson, A. A. Ulyanov, M. I. Petaev, Fine-grained, spinel-rich inclusions from the reduced CV chondrites Efremovka and Leoville: I. Mineralogy, petrology, and bulk chemistry. *Meteor. Planet. Sci.* **39**, 1517–1553 (2004).

57. A. Hashimoto, L. Grossman, SEM-petrography of Allende fine-grained inclusions, in *Proceedings of the 16th Lunar Planetary Science Conference* (1985), Houston, Texas, 11 to 15 March 1985, pp. 323–324.

58. A. Trinquier, J.-L. Birck, C. J. Allegre, Widespread 54Cr heterogeneity in the inner solar system. *Astrophys. J.* **655**, 1179–1185 (2007).

59. K. J. R. Rosman, P. D. P. Taylor, Isotopic compositions of the elements 1997 (Technical Report). *Pure Appl. Chem.* **70**, 217–235 (1998).

60. B. L. A. Charlier, C. Ginibre, D. Morgan, G. M. Nowell, D. G. Pearson, J. P. Davidson, C. J. Ottley, Methods for the microsampling and high-precision analysis of strontium and rubidium isotopes at single crystal scale for petrological and geochronological applications. *Chem. Geol.* **232**, 114–133 (2006).

61. K. R. Ludwig, Isoplot/Ex Version 2.49: A geochronological toolkit for Microsoft Excel (Berkeley Chronology Center, Berkeley, CA, 2002).

62. E. Rotenberg, D. W. Davis, Y. Amelin, S. Ghosh, B. A. Bergquist, Determination of the decay-constant of 87Rb by laboratory accumulation of 87Sr. *Geochim. Cosmochim. Acta* **85**, 41–57 (2012).

63. N. Dauphas, A. Pourmand, Thulium anomalies and rare earth element patterns in meteorites and Earth: Nebular fractionation and the nugget effect. *Geochim. Cosmochim. Acta* **163**, 234–261 (2015).

64. R. T. M. Marquez, B. L. A. Charlier, F. L. H. Tissot, Search for the carriers of anomalous nucleosynthetic signatures in early solar system condensates, in *Proceedings of the 52nd Lunar Planetary Science Conference* (2021), 15 to 19 March 2021, id. 2635.

Citation: B. L. A. Charlier, F. L. H. Tissot, H. Vollstaedt, N. Dauphas, C. J. N. Wilson, R. T. Marquez, Survival of presolar p-nuclide carriers in the nebula revealed by stepwise leaching of Allende refractory inclusions. *Sci. Adv.* **7**, eabf6222 (2021).

Science Advances

Survival of presolar *p*-nuclide carriers in the nebula revealed by stepwise leaching of Allende refractory inclusions

Bruce L. A. Charlier, François L. H. Tissot, Hauke Vollstaedt, Nicolas Dauphas, Colin J. N. Wilson and Ren T. Marquez

ARTICLE TOOLS	http://advances.sciencemag.org/content/7/28/eabf6222
SUPPLEMENTARY MATERIALS	http://advances.sciencemag.org/content/suppl/2021/07/02/7.28.eabf6222.DC1
REFERENCES	This article cites 55 articles, 4 of which you can access for free http://advances.sciencemag.org/content/7/28/eabf6222#BIBL
PERMISSIONS	http://www.sciencemag.org/help/reprints-and-permissions

Use of this article is subject to the Terms of Service